Published in final edited form as:
Exp Eye Res. 2012 August ; 101: 60–71. doi:10.1016/j.exer.2012.05.013.

Pathological Consequences of Long-Term Mitochondrial Oxidative Stress in the Mouse Retinal Pigment Epithelium

Soo-jung Seo, Ph.D., **Mark P. Krebs, Ph.D.**[1], **Haoyu Mao, Ph.D.**, **Kyle Jones**, **Mandy Conners**, and **Alfred S. Lewin, Ph.D.**
Department of Molecular Genetics and Microbiology, University of Florida, Gainesville, FL 32610

Abstract

Oxidative stress in the retinal pigment epithelium (RPE) is hypothesized to be a major contributor to the development of age-related macular degeneration (AMD). Mitochondrial manganese superoxide dismutase (MnSOD) is a critical antioxidant protein that scavenges the highly reactive superoxide radical. We speculated that specific reduction of MnSOD in the RPE will increase the level of reactive oxygen species in the retina/RPE/choroid complex leading to pathogenesis similar to geographic atrophy. To test this hypothesis, an *Sod2*-specific hammerhead ribozyme (Rz), delivered by AAV2/1 and driven by the human *VMD2* promoter was injected subretinally into C57BL/6J mice. Dark-adapted full field electroretinogram (ERG) detected a decrease in the response to light. We investigated the age-dependent phenotypic and morphological changes of the outer retina digital fundus imaging and SD-OCT measurement of ONL thickness. Fundus microscopy revealed pigmentary abnormalities in the retina and these corresponded to sub-retinal and sub-RPE deposits seen in SD-OCT B-scans. Light and electron microscopy documented the localization of apical deposits and thickening of the RPE. In RPE flat-mounts we observed abnormally displaced nuclei and regions of apparent fibrosis in the central retina of the oldest mice. This region was surrounded by enlarged and irregular RPE cells that have been observed in eyes donated by AMD patients and in other mouse models of AMD.

Keywords

retinal pigment epithelium; oxidative stress; superoxide dismutase; mitochondria; mouse model; age related macular degeneration

1. Introduction

Age-related macular degeneration (AMD) is one of the most common irreversible causes of severe loss of vision in developed countries (Cheung, Tai, Kawasaki, Tay, Lee, Hamzah and Wong, 2011;Klein, Chou, Klein, Zhang, Meuer and Saaddine, 2011;Krishnan, Ravindran, Murthy, Vashist, Fitzpatrick, Thulasiraj, John, Maraini, Camparini, Chakravarthy and Fletcher, 2010;Minassian, Reidy, Lightstone and Desai, 2011;Rudnicka, Jarrar, Wormald, Cook, Fletcher and Owen, 2011). The disease is first recognized by the formation of acellular deposits below the retinal pigmented epithelium (RPE) known as *drusen*, which are strongly associated with later RPE atrophy or neovascular changes leading to macular

[1]Current address: The Jackson Laboratory, Bar Harbor, ME 04609

edema and hemorrhage. These events eventually destroy the macula, which is the portion of the central retina needed for seeing objects clearly for common daily tasks such as reading and driving. Two forms of the disease are recognized, dry AMD, and neovascular, or wet AMD. Dry AMD usually refers to the accumulation of macular drusen that may not initially impair vision, though the late-stage, known as geographic atrophy, is associated with degeneration of photoreceptors. The wet form of AMD is characterized by macular edema and hemorrhage, and is often the first clinical manifestation apparent to patients, as a sudden loss of central vision. The pathophysiology of AMD is complex and includes genetic, environmental and immunological factors(Swaroop, Chew, Bowes Rickman and Abecasis, 2009).

Oxidative stress in the retinal pigment epithelium (RPE) is hypothesized to be a major contributor to the development of age-related macular degeneration (AMD)(Beatty, Koh, Phil, Henson and Boulton, 2000;Cai, Nelson, Wu, Sternberg, Jr. and Jones, 2000;Crabb, Miyagi, Gu, Shadrach, West, Sakaguchi, Kamei, Hasan, Yan, Rayborn, Salomon and Hollyfield, 2002;Shen, Dong, Hackett, Bell, Green and Campochiaro, 2007;Totan, Yagci, Bardak, Ozyurt, Kendir, Yilmaz, Sahin and Sahin, 2009). Tobacco smoke, a major environmental risk factor for AMD, is a rich source of oxidants (Cano, Thimmalappula, Fujihara, Nagai, Sporn, Wang, Neufeld, Biswal and Handa, 2010;Fletcher, 2010;Jia, Liu, Sun, Miller, Ames, Cotman and Liu, 2007;Khan, Thurlby, Shahid, Clayton, Yates, Bradley, Moore and Bird, 2006). In contrast, dietary antioxidants reduce the progression of the disease(Seddon, Ajani, Sperduto, Hiller, Blair, Burton, Farber, Gragoudas, Haller, Miller and ., 1994) Mitochondria are thought to be the major source of endogenous reactive oxygen species (ROS), since approximately 2% of NADH-derived electrons are transferred to molecular oxygen rather than to ubiquinone by Complex I of the respiratory chain, and this transfer results in the formation of the highly reactive superoxide anion(Turrens and Boveris, 1980). Superoxide is also a byproduct of electron transfer by Complex III. Mitochondria contain small molecules, such as glutathione, and enzymes to scavenge or convert superoxide into less dangerous molecules. Mitochondrial manganese superoxide dismutase (MnSOD) is a critical antioxidant protein that reduces superoxide radical to hydrogen peroxide(Klug, Rabani and Fridovich, 1972). Hydrogen peroxide is converted to water by glutathione peroxidase, or, outside the mitochondrion, by catalase. We reasoned that specific reduction of MnSOD in the RPE will increase the level of reactive oxygen species in the retina/RPE/choroid complex leading to pathogenesis of the early signs of AMD.

The role of MnSOD in AMD and RPE pathology has been explored by genetic studies in human populations and in mouse models. Kimura et al. reported an association between a polymorphism in the leader sequence of *SOD2* and exudative AMD (Kimura, Isashiki, Sonoda, Kakiuchi-Matsumoto and Ohba, 2000). However, this finding was not replicated by another group in Japan (Kondo, Bessho, Honda and Negi, 2009) or in an Irish population(Esfandiary, Chakravarthy, Patterson, Young and Hughes, 2005). Nevertheless, *Sod2* knockout mice show retinal abnormalities including accumulation of swollen mitochondria in the RPE (Sandbach, Coscun, Grossniklaus, Kokoszka, Newman and Wallace, 2001). These mice die as neonates, so that the long-term effect of mitochondrial oxidative stress in the RPE cannot be studied in them. $Sod1^{-/-}$ mice, which lack cytoplasmic CuZn superoxide dismutase, live longer and exhibited some features of AMD, such as sub-RPE structures similar to drusen, choroidal neovascularization, and retinal pigment epithelium dysfunction when mice were older than seven months, though a consistent phenotype required exposure to constant light for 24 hours (Imamura, Noda, Hashizume, Shinoda, Yamaguchi, Uchiyama, Shimizu, Mizushima, Shirasawa and Tsubota, 2006).

In an effort to increase oxidative stress only in the RPE, as opposed to systemic oxidative stress as in *Sod1* and *Sod2* knockout mice, we previously tested the subretinal injection of AAV2/1 expressing the *Sod2*-specific ribozyme Rz432 from a non-specific promoter in C57BL/6J mice and DBA/1J mice (Justilien, Pang, Renganathan, Zhan, Crabb, Kim, Sparrow, Hauswirth and Lewin, 2007). By six months post-injection these mice developed phenotypes analogous to those seen in patients with geographic atrophy including reduction of scoptopic (dark adapted) electroretinogram (ERG) response, vacuolization of the RPE, thickening of Bruch's membrane, shortening and disorganization of the photoreceptor outer and inner segments, and increased autofluorescence and elevated levels of A2E. To improve this strategy, we used the RPE-specific *VMD2* (*BEST1*) promoter to express Rz432 in the RPE via an AAV vector and examined long-term phenotypes using fundus imaging and spectral domain optical coherence tomography (SD-OCT) in living mice, as well as light and electron microscopic analysis of the retina and RPE following sacrifice.

2. Materials and Methods

2.1 Mice and AAV Injections

Four-week-old C57BL/6J mice were injected with AAV2/1 expressing *Sod2*-specific hammerhead ribozyme Rz432 (Qi, Lewin, Hauswirth and Guy, 2003) from the RPE specific human *VMD2* promoter and GFP from the CMV immediate early promoter (Supplemental Fig. 1). Ten minutes before the injections, 1% atropine sulfate solution was placed topically on the eyes of the mice. The mice were anesthetized using ketamine/xylazine solution as previously described. Right eyes were injected subretinally with 1.0 μl of 2.5×10^{12} particles/ml of AAV-ribozyme (AAV-Rz432-*gfp*) and left eyes were either uninjected or injected with a similar amount of AAV-*gfp* as a control. In the control virus, GFP synthesis was programmed by the CMV enhancer and the chicken β-actin promoter (CBA promoter). Using a Nikon SM2800 operating microscope (Nikon, Melville, NY), a 28 gauge hypodermic needle was used to puncture the cornea to create an aperture. A blunt 32 gauge needle on a Hamilton syringe was inserted through the hole and vector was injected into the subretinal space.

2.3.Fundus Analysis

A Micron III retinal imaging microscope (Phoenix Research Laboratories, Pleasanton, CA) was used to monitor pathological changes in the fundus. Mice were anesthetized by intraperaitoneal (IP) injection of ketamine/xylazine mixture (0.1μl/20g mouse) and eyes were dilated with 1.0% atropine. The vibrissae were trimmed with fine scissors to prevent them from obscuring the photograph. The mouse was held on its side on the microscope platform. Focusing was achieved by moving the mouse. The mouse position and angle were altered to study different parts of the fundus. For angiography, fluorescein (0.02 ml of 25%, Hub Pharmaceuticals, Rancho Cucamonga, CA) was delivered once through intraperitoneal injection. One minute after injection, images were acquired every minute until the fluorescein was clearly visible and then at 2 minute intervals thereafter. Fundus images were produced for six mice at 12 months post injection and for another six mice at 18 months. Representative images are presented.

2.4. Electroretinographic Analysis

For dark-adapted ERGs, animals were dark adapted overnight prior to analysis, and all procedures were performed under dim red light. The mice were anesthetized by IP injection of a mixture of ketamine and xylazine, and eyes were dilated with 1.0% atropine. Gold contact lens electrodes were placed on the eyes with 1% methylcellulose, a reference electrode was placed subcutaneously between the shoulder blades and a ground electrode subcutaneously in a hind leg. The mice were placed on a heated platform with their heads

completely inside a Ganzfeld illumination dome. Full-field ERGs were obtained in the dark adapted state by flashing increasing intensities of light (0.02, 0.18 and 2.68 cds/m2) into the eyes of the mice. The electrical responses of the retinas were recorded simultaneously from both eyes using the UTAS-E 2000 Visual Electrodiagnostic System. Intervals between flashes (15 to 60 seconds) were increased with increasing flash intensities. Five recordings were taken and averaged per flash intensity. A group of five mice was analyzed at nine months post injection and another group of 10 mice was analyzed at twelve months post injection.

2.5. Electron Microscopy

For electron microscopy, four mice from each treatment group were given an overdose of sodium pentobarbital and then immediately perfused with 4% paraformaldehyde and 2% glutaraldehyde in 0.1 M phosphate-buffered saline (PBS) pH 7.4. The eyes were removed and immersed in 4% paraformaldehyde and 2% glutaraldehyde for further fixation overnight. Eyes were postfixed with 1% osmium tetroxide, 0.1 M sodium cacodylate-HCl buffer (pH 7.4), and dehydrated through a series of increasing ethanol concentrations leading up to propylene oxide. Eyes were embedded in epoxy resin which was polymerized at 60 °C. For morphometric measurements, 1 μm thick sections were cut along a vertical meridian containing the optic nerve. Sections of 80 to 100 nm were cut and examined by transmission electron microscopy.

2.6. Optical Coherence Topomology

Spectral domain OCT (SD-OCT) provides high resolution analysis of retinal architecture previously achieved only through histology. Using a Bioptigen SD-OCT (Bioptigen, Research Triangle Park, NC), we measured thickness of the outer nuclear layer (ONL) between the outer plexiform layer (OPL) and the external limiting membrane (ELM) using six mice at 12 months and another group of six mice at 18 months post injection. The OPL appeared as a light stripe and the ELM as a very thin light stripe. SD-OCT was also used to identify irregularities in the RPE. Mice were anesthetized by IP injection of ketamine/xylazine mixture (0.1ml/20g mouse) and eyes were dilated with 1.0% atropine. 1000 linear A-scans were used to produce each horizontal B-scan, and 20 B-scans were averaged to minimize the background and to achieve higher resolution. To produce surface images of the fundus, a rectangular volume of 100 B-scans was obtained and analyzed. ONL thickness was measured manually by using the distance measuring tool of InVivoVue, the system software. We recorded four measurements at the same distance from the optical nerve head from each eye and used these data to determine the average final ONL thickness.

2.7. RPE Flat Mount Morphological Analysis

Mice were euthanized by overdose injection of ketamine/xylazine mixture, eyes were enucleated and the cornea, lens and neural retina were removed. For antibody staining, eyecups were fixed with 4% paraformaldehyde for 1 hour at room temperature followed by immersion in ice-cold methanol for 1 hr. Eyecups were then rinsed in PBS and pre-incubated in 10% normal goat serum for 1 hour. The eyecups were incubated overnight in rabbit anti-ZO-1 antibody at 1:500 (Invitrogen) for two hours in fluorophore-conjugated secondary antibody at 1:500 (Invitrogen). After rinses in PBS, four radial cuts were made and the eyecups were flattened and mounted on glass slides in Vectashield mounting medium with 4,6-diamino-2-phenylindole (DAPI; Vectashield;Vector Laboratories, Burlingame, CA). The images were taken with a confocal microscope. To assess morphological changes in the RPE, the anterior eye was removed by dissection and the neural retina separated from the RPE/choroid/sclera complex as described (Krebs, White and Kaushal, 2009). The RPE/choroid/sclera complex was stained overnight with phalloidin Alexafluor 488 (Invitrogen) and DAPI (Sigma-Aldrich) diluted 1:3000 in PBS, rinsed, and

mounted as described above. Flat mounts were imaged by using a 10x objective on a PerkinElmer Ultraview Vox Confocal Imaging with manual or automated movement of the specimen stage to tile the entire sample. At each tile position, a z-stack 5 μm step size, 20 steps was collected. Merged stacks were stitched (Preibisch, Saalfeld and Tomancak, 2009) in Fiji (http://fiji.sc/wiki/index.php/Fiji). A custom macro to divide merged stacks with an averaged and polynomial-fit background image was used to correct for uneven background illumination in the red channel. Three flat mounts were prepared from ribozyme injected eyes and three from control eyes at 23 months post injection.

2.8 Statistical Methods

ERG and SD-OCT data were evaluated using Student's *t* test for paired samples, comparing ribozyme treated-eyes with control treated eyes of the same mice. ANOVA with Bonferroni correction was used for multiple comparisons. Results are expressed as mean±standard error of the mean. $p < 0.05$ was considered statistically significant.

3. Results

3.1. Reduction of Electrophysiological Responses

Our objective was to determine if RPE specific knockdown of MnSOD was sufficient to cause retinal disease similar to geographic atrophy. Although we have previously shown that subretinal delivery of an *Sod2*-specific ribozyme led to a decrease in the scotopic electroretinogram response, we postulated that the same ribozyme driven by the RPE-specific *VMD2* promoter would lead to a similar response. Three-week-old C57BL/6 mice were injected subretinally with AAV1 expressing *VMD2-Rz432* in the right eyes. As a control, left eyes were injected with AAV1 expressing GFP or mCherry from the CBA promoter. As in our earlier experiments, AAV delivery of the *Sod2* ribozyme led to a 50% reduction in the level MnSOD in the RPE compared to control injected eyes (Supplemental Fig. 2). Loss of a- and b-wave response was observed between three and six months post-injection (Fig. 1). By nine months post-injection, an average decrease of ~50% in a-wave amplitudes and ~30% in b-wave amplitudes were observed compared to control-injected eyes. By 12 months post-injection, an ~50% decrease in amplitude was measured for both a- and b-waves. Since this decrease was not substantially different than that seen at six months (Supplemental Fig. 2), we speculate that the impact of the AAV ribozyme is stationary: RPE cells that are infected lost function and lead to photoreceptor death, but other portions of the retina remained intact.

3.2. *Sod2* Knockdown Leads to Fundus Abnormalities

Geographic atrophy (GA) is characterized by the development of areas of outer retinal atrophy that slowly enlarge over time. GA is clinically defined using fundus photography as a defined area of reduced pigmentation with visible choroidal blood vessels and no appearance of choroidal neovascularization (Göbel, Fleckenstein, Schmitz-Valckenberg, Brinkmann and Holz, 2011). By scanning laser ophthalmoscopy, GA is characterized as extinguished autofluorescence in regions of RPE atrophy surrounded by areas of increased autofluorescence, suggestive of increased lipofuscin accumulation (Göbel, Fleckenstein, Schmitz-Valckenberg, Brinkmann and Holz, 2011;Smith, Chan, Busuoic, Sivagnanavel, Bird and Chong, 2006). As early as one month after AAV-Rz432 injection in the eyes of C57Bl/6 mice, hypopigmented regions, suggestive of retinal atrophy were apparent (Fig. 2). By seven months post-injection, discrete refractive foci and perivascular areas of apparent atrophy were evident. There was little change in the extent of focal lesions from this time up to 23 months when the last of the injected mice was sacrificed, again suggesting that this was a stationary, rather than progressive phenotype. As in GA, regions of atrophy in ribozyme-injected eyes were hyperfluorescent when imaged by the fundus camera using

blue excitation and yellow emission filters. However, since this filter combination would also detect fluorescence due to GFP expressed by the recombinant virus, we cannot conclude that the fluorescence observed is attributable to lipofuscin autofluorescence (Supplemental Fig. 3). Nevertheless, in AAV-GFP injected eyes, green fluorescence but no atrophy can be seen, except at the site of subretinal injection (arrow). We have previously shown that AAV delivery of Rz432 leads to accumulation of autofluorescent material in the RPE and to an increase in bisretinoids A2E and iso-A2E (Justilien, Pang, Renganathan, Zhan, Crabb, Kim, Sparrow, Hauswirth and Lewin, 2007).

3.3. Tortuosity of Retinal Blood Vessels Resulting from *Sod2* Knockdown

Fluorescein angiography of Rz432-treated mice showed that the blood vessels in ribozyme-treated eyes exhibited a tortuous appearance (Fig. 3, top). Control injected eyes showed a radial pattern of retina vessels typical of mice. Tortuosity of retinal blood vessels is a typical diagnostic indicator for a number of retinal pathologies (Dougherty, Johnson and Wiers, 2010) and may be related to the up-regulation of VEGF(Tee, Penrose, O'Shea, Lai, Rakoczy and Dunlop, 2008). In addition, focal loss of capillaries was noted in Rz-432 treated eyes (arrowheads). We also observed what appeared to be extravascular leakage of fluorescein, and because of the short exposure time of this diffuse staining was probably unrelated to GFP. Diffuse staining was not observed in controlled injected eyes. However, upon time-lapse photography of ribozyme and control injected eyes (Fig. 3, bottom) we saw no change in the pattern of green fluorescence with time. Therefore, we conclude that the diffuse fluorescence was caused by scarring or injury but was not associated with leakage of either choroidal or retinal blood vessels. In other angiograms (Supplemental Fig. 4) we observed evidence of venous beading and possible microaneurysms. These fluorescein-labeled foci did not change with increasing time, suggesting no active bleeding.

3.4. ONL Thinning and Subretinal Deposits Revealed by SD-OCT

We used spectral domain optical coherence tomography (SD-OCT) to examine areas of apparent atrophy seen in the digital fundus images (Fig. 4A). We obtained approximate alignment by obtaining *en face* images of the retina by SD-OCT, and using the retinal vascular as guides. Transverse B-scans were performed across hypopigmented regions of the retina (Fig 4B). In some regions of the scan we observed thinning of the ONL, but no irregularities in the RPE layer. Toward the center of the retina, SD-OCT revealed deposits beneath the photoreceptor layer resembling SD-OCT images of reticular pseudodrusen seen in AMD patients (small arrows Fig. 4D and E) (Zweifel, Imamura, Spaide, Fujiwara and Spaide, 2010). We also observed a less refractile (possibly fluid filled) region beneath the retina (large arrow in Fig. 4D) and a subretinal deposit asociatred with deformation of the inner layers of the retina (large arrow in Fig. 4E).. The thickness of the outer nuclear layer (ONL) was also measured by SD-OCT, using the inner plexiform layer and the external limiting membranes as landmarks. By 12 months post-injection of AAV-Rz432, we measured an average decrease of 23% in ONL thickness in Rz432-treated eyes compared to control-treated eyes ($p<0.001$) (Fig. 5). In another group of mice, the same difference in ONL thickness was measured at 18 months post-injection (Supplemental Fig. 5).

3.5 Microscopic Abnormalities in the RPE

While our SD-OCT images could not distinguish between subretinal and sub-RPE deposits, light microscopic inspection of toluidine blue-stained sections (Fig. 6) suggest that the deposits we observed lie within the RPE as well as between the RPE and the photoreceptors (Fig. 6B). The RPE was thickened in the ribozyme treated eyes, and this distention was pan-retinal (Fig. 6C). Our earlier work using AAV-Rz432 demonstrated that knockdown of MnSOD led to an accumulation of basal laminar deposits within the RPE by four months post injection, and this accumulation may account for the distension of the RPE seen here.

However, we also noticed deposits on the apical surface of the RPE (arrow in Fig. 6B). In the RPE of ribozyme treated retinas, we frequently observed swelling and fragmentation of mitochondria (Fig. 7B), and this was never seen in the RPE of eyes injected with AAV-GFP (Fig. 7A). Organelles appeared to lose electron density and had a reduced number of cristae compared to mitochondria in control-treated RPE. We also observed what appeared to be autophagosomes containing membrane bounded vesicles in eyes injected with AAV-Rz432 (Fig. 7D), and these were not observed in the control-injected eyes (Fig. 7C). Lipofuscin vesicles were detected in both ribozyme treated and control eyes, and there did not seem to be an increase in these vesicles based on electron microscopy, though we have reported an increase in both autofluorescence and in the accumulation of bisretinoids following depletion of MnSOD in the RPE (Justilien, Pang, Renganathan, Zhan, Crabb, Kim, Sparrow, Hauswirth and Lewin, 2007;Thampi, Rao, Mitter, Cai, Mao, Li, Seo, Qi, Lewin, Romano and Boulton, 2012). In addition, as noted in our earlier work, Bruch's membrane (BM) appeared thickened and disorganized (Fig. 7F) compared to the laminar structure of Bruch's membrane in the control treated RPE (Fig. 7F). .

3.5. RPE Atrophy Revealed in Flat Mounts

Although histological and ultrastructural imaging of the RPE in cross-section provided evidence of dystrophic changes, we wondered whether *en face* imaging might provide more information of the regional distribution of the pathology. Ding *et al.*, using an AMD model based on feeding APOE4 knock-in mice a high fat high cholesterol diet, reported that RPE cells were enlarged and more frequently multinucleate in mice fed the high fat diet for a year as opposed to genetically equivalent mice fed normal chow (Ding, Johnson, Herrmann, Farsiu, Smith, Groelle, Mace, Sullivan, Jamison, Kelly, Harrabi, Bollini, Dilley, Kobayashi, Kuang, Li, Pons, Lin and Rickman, 2011). Al-Hussaini *et al.* reported similar change associated with drusen in eyes of AMD patients (Al-Hussaini, Schneiders, Lundh and Jeffery, 2009). To determine if similar changes occur as a consequence of *Sod2* knockdown, we stained RPE/choroid/sclera flat mounts using an antibody against ZO-1 (zona occludins 1) to visualize RPE tight junctions and the outline of RPE cells. Staining in the *VMD2-Rz432* injected RPE showed that individual RPE cells frequently became enlarged and binucleated as reported by Ding and coworkers (Fig. 8). Strikingly, the nuclei of RPE cells appeared condensed and at the cell periphery.

Indeed, in flat mounts of RPE from older mice (23 months), in the area of AAV injection, we observed areas in which phalloidin-stained polygonal cells were absent and replaced with numerous smaller cells that did not express GFP (Fig. 9). These cells were surrounded by a transition zone of phalloidin-positive but enlarged, irregular RPE cells and by GFP-positive RPE cells of normal morphology. Surrounding this region were GFP-negative cells of normal RPE morphology. We interpret the proliferation of small cells in the center of the retina as fibrosis replacing lost RPE cells. Such localized scarring is typical in the late stages of AMD. RPE flat mounts of the uninjected contralateral eyes did not show dropout of RPE cells or fibrotic regions (supplemental Fig. 6).

4. Discussion

The hypothesis that we tested is that an increase in mitochondrial oxidative stress in the RPE of mice will lead to some of the pathologies characteristic of age related macular degeneration. In our earlier work (Justilien, Pang, Renganathan, Zhan, Crabb, Kim, Sparrow, Hauswirth and Lewin, 2007), we also used AAV to deliver a ribozyme targeting *Sod2* mRNA in the RPE and demonstrated a significant increase in oxidative stress in the retina as a result of MnSOD reduction in the RPE. Oxidative stress led to a decline in scotopic ERG amplitudes accompanied by a thinning of the outer nuclear layer. This impact on photoreceptors was associated with RPE pathology including the accumulation of

autofluorescent foci, an increase in bisretinoids such as A2E, vacuolization of the RPE and disorganization of Bruch's membrane.

In the current work, we improved upon both the methodology and the analysis, however, our results completely substantiate those reported by Justilien et al. In the experiments reported here, we utilized the RPE-specific *VMD2* (Bestrophin) promoter instead of cytomegalovirus β-actin (CBA) promoter to direct production of the *Sod2* ribozyme and employed some of the same imaging technology used to diagnose AMD clinically (digital fundus imaging, angiography and spectral domain optical coherence tomography). Levels of MnSOD in the RPE were reduced by approximately 50% both in our earlier work with the CBA promoter and in these experiments using the *VMD2* promoter to drive ribozyme expression. Based on the extent of GFP transduction in the RPE (Supplemental Fig. 4), we infected 60–70% of the retina with AAV, suggesting that the reduction in MnSOD was much greater than 50% in those cells infected by virus. The in-life methods, backed up by *post mortem* histology and electron microscopy, indicated that MnSOD knockdown in the RPE does recapitulate some clinical features of AMD including abnormalities in RPE pigment, subretinal deposits reminiscent of reticular pseudodrusen, and accumulation of debris within the RPE itself. We did not observe evidence of choroidal neovascularization or of large sub-RPE deposits. As in our previous work, RPE injury was associated with loss of photoreceptors and a decline in scotopic ERG amplitudes. We did not measure an increase in lipofuscin content in this set of experiments, but an increase in autofluorescence seems to be a conisistent feature of this model (Thampi, Rao, Mitter, Cai, Mao, Li, Seo, Qi, Lewin, Romano and Boulton, 2012).

The retinal atrophy we observed was geographic, if artificially so: it occurred where we placed the virus, based on the coincidence of atrophy with expression of GFP carried by the AAV-ribozyme (Supplemental Fig. 4). Retinal pigment was depleted in these regions (Fig. 2), and hypopigmented areas were frequently associated with abnormalities in the RPE detected in the SD-OCT B-scans (Fig. 4). SD-OCT and digital fundus photography are quite different imaging techniques, operating at different wave lengths, and there was not absolute coincidence between fundus blemishes and hyper-reflective elements detected by SD-OCT. Sohrab *et al.* have recently described approach to registration of different imaging modalities in order to characterize reticular pseudodrusen(Sohrab, Smith, Salehi-Had, Sadda and Fawzi, 2011). Microscopy of fixed tissue should help identify the sources of the retinal abnormalities detected in living animals, but our challenge has been identifying regions of interest once the tissue is stained with OsO_4 and embedded in plastic for tissue sectioning. The fundus and SD-OCT images we studied were restricted to the central third of the retina, and the optic nerve head and retinal vasculature should provide useful landmarks.

Fluorescein angiography revealed another phenotype of RPE knockdown of MnSOD: retinal blood vessels often appeared tortuous. We saw evidence of microaneurisms in some eyes (Supplemental Fig. 4). The tortuosity of retinal blood vessels is a diagnostic indicator for a number of retinal pathologies including diabetic retinopathy and retinopathy of prematurity (ROP)(Dougherty, Johnson and Wiers, 2010). Up-regulation of vascular endothelial growth factor (VEGF) in a diabetic retinopathy induces retinal vascular damage such as microaneurysms, hemorrhage, venous beading and tortuosity and loops in the arteries and veins(Tee, Penrose, O'Shea, Lai, Rakoczy and Dunlop, 2008). We measured VEGF levels in whole retinas by ELISA one month after virus injection, but we did not detect a difference between retinas injected with AAV-Rz and those injected with AAV-GFP (data not shown). Metabolic abnormalities of diabetes can cause an increase in mitochondrial superoxide production (Giacco and Brownlee, 2010). Since the AAV-ribozyme treatment was intended to increase superoxide accumulation by mitochondria, these vascular changes could be a response to RPE oxidative stress.

SD-OCT was useful in documenting thinning of the ONL in living animals and for identifying deposits within and on top of the RPE. While we did not observe massive sub-RPE deposits, the subretinal deposits that we detected were similar to the sub-retinal drusenoid deposits (reticular pseudodrusen) commonly seen in people with AMD (Cohen, Dubois, Tadayoni, Delahaye-Mazza, Debibie and Quentel, 2007). Sub-retinal drusenoid deposits contain many of the same components as drusen including unesterified cholesterol, vitronectin, apoE and complement factor H (Rudolf, Malek, Messinger, Clark, Wang and Curcio, 2008). They do not contain apoB, apoA1 and esterified cholesterol typically found in sub-RPE drusen. We have not characterized the molecular composition of the subretinal deposits we identified, but this will a goal of future research.

The Bowes-Rickmann group has demonstrated the utility of RPE flat mounts in characterizing AMD-like pathology in the mouse and AMD pathology in humans. Using mice expressing human *APOE4* in place of the endogenous gene and fed a high-fat, high-cholesterol diet, they used ZO-1 stained flat mounts to describe the presence of unusually large RPE cells that were not found in genetically identical mice fed a normal diet(Ding, Johnson, Herrmann, Farsiu, Smith, Groelle, Mace, Sullivan, Jamison, Kelly, Harrabi, Bollini, Dilley, Kobayashi, Kuang, Li, Pons, Lin and Rickman, 2011). This group developed a system of morphometry to measure the presence of enlarged cells quantitatively. They then demonstrated that systemic administration of antibodies to Aβ40 and Aβ42 to the mice reduced the presence of the abnormal cells and also reduced the basal laminar deposits and thickening of Bruch's membrane detected in RPE cross sections. Our analysis of flat mounts has not been quantitative, but we also observed changes in the size and displacement of RPE cells as detected by ZO-1 and phalloidin staining (Figs. 8 and 9). We also noted regions of enlarged and irregular RPE cells. These bordered a central region of apparent fibrosis, in which RPE cells have been replaced with smaller cells of fibroblastic morphology. Confirming their identify will require staining with fibroblast markers, but such scarring is characteristic of late stage AMD. While disciform scars are a consequence of neovascular AMD, fibrotic lesions are not typically found in geographic atrophy.

There are other mouse models of AMD-like pathology based on oxidative stress or mitochondrial deficiency. Mice disrupted for *Sod1*, the gene for Cu/Zn superoxide dismutase, accumulate sub-RPE deposits and show signs of choroidal neovascularization in older animals(Dong, Xie, Shen, Yoshida, Yokoi, Hackett and Campochiaro, 2009;Imamura, Noda, Hashizume, Shinoda, Yamaguchi, Uchiyama, Shimizu, Mizushima, Shirasawa and Tsubota, 2006). Mice deficient in the transcription factor NRF2, which stimulates the expression of genes involved in the antioxidant response, exhibit RPE degeneration with accumulation of lipofuscin, drusen-like deposits and choroidal neovascularization, suggesting that oxidative stress in the RPE leads to an AMD-like pathology(Zhao, Chen, Wang, Sternberg, Freeman, Grossniklaus and Cai, 2011). Unlike our model, the oxidative stress in these models is systemic. Zhou et al.(Zhao, Yasumura, Li, Matthes, Lloyd, Nielsen, Ahern, Snyder, Bok, Dunaief, LaVail and Vollrath, 2011) described a model in which the mitochondrial transcription factor TFAM was depleted in the RPE, resulting in loss of oxidative phosphorylation in these cells. The eyes of these mice exhibited some of the same damage to the RPE and photoreceptors that we report, but they also noted sub-RPE drusen-like deposits. They went on to show that the AKT/mTOR pathway was involved with the de-differentiation of RPE cells in this model and these effects could be mitigated by administration of rapamycin.

The advantage of the AAV-*Sod2* ribozyme model for retinal degeneration is that it is RPE-directed and is associated with an accepted risk factor of AMD, namely oxidative stress. Injury to the RPE and overlying retina is local, based on the displacement of the virus, but occurs in every injected eye beginning by two months post-injection. The presence of a

contralateral control eye provides an important internal control, especially with for ERG measurements, which may vary considerably between mice. Disadvantages of this model include the fact that frank drusen and choroidal neovascularization were not observed and that subretinal injection of AAV caused localized injury. For this reason, we are working on a model in which *Sod2* is deleted in the RPE using the *cre-lox* system. Because genetic blockade of oxidative phosphorylation causes significant RPE damage phosphorylation (Zhao, Yasumura, Li, Matthes, Lloyd, Nielsen, Ahern, Snyder, Bok, Dunaief, LaVail and Vollrath, 2011), it remains to be seen whether the impact on RPE that we have seen is caused by loss of mitochondrial function, by the increase in oxidative stress or by both.

Because it leads to geographic atrophy, this model of oxidative stress in the RPE lends itself to testing of therapies for dry AMD. We recently demonstrated that systemic treatment of mice with 8-hydroxy-2-(di-*n*-propylamino)-tetralin (8-OH DPAT) reduces retinal degeneration resulting from subretinal injection of AAV-VMD2-Rz432(Thampi, Rao, Mitter, Cai, Mao, Li, Seo, Qi, Lewin, Romano and Boulton, 2012), suggesting that 5-hydroxy tryptamine receptor agonists may be effect therapeutic agents for geographic atrophy.. Since this drug appears to stimulate antioxidant defences, either drug treatment or a gene delivery to stimulate an anti-oxidant response, perhaps through the antioxidant response element (ARE), would also seem logical (Ha, Chen, Cai and Sternberg, Jr., 2006;Mandal, Patlolla, Zheng, Agbaga, Tran, Wicker, Kasus-Jacobi, Elliott, Rao and Anderson, 2009;Tanito, Agbaga and Anderson, 2007). Mitochondrial targeted antioxidant compounds may also be effective (Markovets, Fursova and Kolosova, 2011). Alternatively, it may be possible to block the complement related injury resulting from oxidative stress in the RPE (Rohrer, Long, Coughlin, Wilson, Huang, Qiao, Tang, Kunchithapautham, Gilkeson and Tomlinson, 2009;Thurman, Renner, Kunchithapautham, Ferreira, Pangburn, Ablonczy, Tomlinson, Holers and Rohrer, 2009). We did not assess complement activation in these ribozyme treated eyes. However, we are developing a mouse model in which the *SOD2* gene is deleted using the Cre-lox system, and in these mice deposition of complement regulatory protein CD46 and of C5 was observed, enabling testing of agents that limit complement damage to the RPE and retina.

5. Conclusion

We have generated an in vivo model of chronic oxidative stress in the RPE layer of the retina. The oxidative damage-mediated changes in the retina-RPE-choroid complex of these mice lead to AMD-like lesions. Using our mouse model, several therapeutic approaches have been tested. Our AMD model should help to understand the disease mechanism and to test various therapeutic approaches.

Supplementary Material

Refer to Web version on PubMed Central for supplementary material.

Acknowledgments

This research was funded by grants from the Macular Vision Research Foundation, the James and Esther King Biomedical Research Program (1KG08-33981) and the National Eye Institute (5R01EY020825, and P30-EY021721).

Abbreviations

AAV Adeno-Associated Virus

AMD	age related macular degeneration, MnSOD, manganese superoxide dismutase encoded by the *SOD2* gene
ROS	reactive oxygen species
RPE	retinal pigment epithelium
VMD2	vitelliform macular dystrophy 2

References

Al-Hussaini H, Schneiders M, Lundh P, Jeffery G. Drusen are associated with local and distant disruptions to human retinal pigment epithelium cells. Exp Eye Res. 2009; 88:610–2. [PubMed: 18992244]

Beatty S, Koh H, Phil M, Henson D, Boulton M. The role of oxidative stress in the pathogenesis of age-related macular degeneration. Surv Ophthalmol. 2000; 45:115–34. [PubMed: 11033038]

Cai J, Nelson KC, Wu M, Sternberg P Jr, Jones DP. Oxidative damage and protection of the RPE. Prog Retin Eye Res. 2000; 19:205–21. [PubMed: 10674708]

Cano M, Thimmalappula R, Fujihara M, Nagai N, Sporn M, Wang AL, Neufeld AH, Biswal S, Handa JT. Cigarette smoking, oxidative stress, the anti-oxidant response through Nrf2 signaling, and Age-related Macular Degeneration. Vision Res. 2010; 50:652–64. [PubMed: 19703486]

Cheung CM, Tai ES, Kawasaki R, Tay WT, Lee JL, Hamzah H, Wong TY. Prevalence of and Risk Factors for Age-Related Macular Degeneration in a Multiethnic Asian Cohort. Arch Ophthalmol. 2011

Cohen SY, Dubois L, Tadayoni R, Delahaye-Mazza C, Debibie C, Quentel G. Prevalence of reticular pseudodrusen in age-related macular degeneration with newly diagnosed choroidal neovascularisation. Br J Ophthalmol. 2007; 91:354–9. [PubMed: 16973663]

Crabb JW, Miyagi M, Gu X, Shadrach K, West KA, Sakaguchi H, Kamei M, Hasan A, Yan L, Rayborn ME, Salomon RG, Hollyfield JG. From the Cover: Drusen proteome analysis: An approach to the etiology of age-related macular degeneration. Proceedings of the National Academy of Sciences. 2002; 99:14682–7.

Ding JD, Johnson LV, Herrmann R, Farsiu S, Smith SG, Groelle M, Mace BE, Sullivan P, Jamison JA, Kelly U, Harrabi O, Bollini SS, Dilley J, Kobayashi D, Kuang B, Li W, Pons J, Lin JC, Rickman CB. Anti-amyloid therapy protects against retinal pigmented epithelium damage and vision loss in a model of age-related macular degeneration. Proceedings of the National Academy of Sciences. 2011; 108:E279–E287.

Dong A, Xie B, Shen J, Yoshida T, Yokoi K, Hackett SF, Campochiaro PA. Oxidative stress promotes ocular neovascularization. J Cell Physiol. 2009; 219:544–52. [PubMed: 19142872]

Dougherty G, Johnson MJ, Wiers MD. Measurement of retinal vascular tortuosity and its application to retinal pathologies. Med Biol Eng Comput. 2010; 48:87–95. [PubMed: 20012560]

Esfandiary H, Chakravarthy U, Patterson C, Young I, Hughes AE. Association study of detoxification genes in age related macular degeneration. Br J Ophthalmol. 2005; 89:470–4. [PubMed: 15774926]

Fletcher AE. Free radicals, antioxidants and eye diseases: evidence from epidemiological studies on cataract and age-related macular degeneration. Ophthalmic Res. 2010; 44:191–8. [PubMed: 20829643]

Göbel AP, Fleckenstein M, Schmitz-Valckenberg S, Brinkmann CK, Holz FG. Imaging Geographic Atrophy in Age-Related Macular Degeneration. Ophthalmologica. 2011; 226:182–90. [PubMed: 21865677]

Giacco F, Brownlee M. Oxidative Stress and Diabetic Complications. Circ Res. 2010; 107:1058–70. [PubMed: 21030723]

Ha KN, Chen Y, Cai J, Sternberg P Jr. Increased Glutathione Synthesis through an ARE-Nrf2-Dependent Pathway by Zinc in the RPE: Implication for Protection against Oxidative Stress. Investigative Ophthalmology Visual Science. 2006; 47:2709–15. [PubMed: 16723490]

Imamura Y, Noda S, Hashizume K, Shinoda K, Yamaguchi M, Uchiyama S, Shimizu T, Mizushima Y, Shirasawa T, Tsubota K. Drusen, choroidal neovascularization, and retinal pigment epithelium dysfunction in SOD1-deficient mice: a model of age-related macular degeneration. Proc Natl Acad Sci USA. 2006; 103:11282–7. [PubMed: 16844785]

Jia L, Liu Z, Sun L, Miller SS, Ames BN, Cotman CW, Liu J. Acrolein, a Toxicant in Cigarette Smoke, Causes Oxidative Damage and Mitochondrial Dysfunction in RPE Cells: Protection by (R)-{alpha}-Lipoic Acid. Investigative Ophthalmology Visual Science. 2007; 48:339–48. [PubMed: 17197552]

Justilien V, Pang JJ, Renganathan K, Zhan X, Crabb JW, Kim SR, Sparrow JR, Hauswirth WW, Lewin AS. SOD2 knockdown mouse model of early AMD. Invest Ophthalmol Vis Sci. 2007; 48:4407–20. [PubMed: 17898259]

Khan JC, Thurlby DA, Shahid H, Clayton DG, Yates JRW, Bradley M, Moore AT, Bird AC. Smoking and age related macular degeneration: the number of pack years of cigarette smoking is a major determinant of risk for both geographic atrophy and choroidal neovascularisation. Br J Ophthalmol. 2006; 90:75–80. [PubMed: 16361672]

Kimura K, Isashiki Y, Sonoda S, Kakiuchi-Matsumoto T, Ohba N. Genetic association of manganese superoxide dismutase with exudative age-related macular degeneration. Am J Ophthalmol. 2000; 130:769–73. [PubMed: 11124296]

Klein R, Chou CF, Klein BE, Zhang X, Meuer SM, Saaddine JB. Prevalence of age-related macular degeneration in the US population. Arch Ophthalmol. 2011; 129:75–80. [PubMed: 21220632]

Klug D, Rabani J, Fridovich I. A direct demonstration of the catalytic action of superoxide dismutase through the use of pulse radiolysis. J Biol Chem. 1972; 247:4839–42. [PubMed: 4626367]

Kondo N, Bessho H, Honda S, Negi A. SOD2 gene polymorphisms in neovascular age-related macular degeneration and polypoidal choroidal vasculopathy. Molecular Vision. 2009; 15:1819–26. [PubMed: 19753309]

Krebs MP, White DA, Kaushal S. Biphasic Photoreceptor Degeneration Induced by Light in a T17M Rhodopsin Mouse Model of Cone Bystander Damage. Invest Ophthalmol Vis Sci. 2009

Krishnan T, Ravindran RD, Murthy GV, Vashist P, Fitzpatrick KE, Thulasiraj RD, John N, Maraini G, Camparini M, Chakravarthy U, Fletcher AE. Prevalence of early and late age-related macular degeneration in India: the INDEYE study. Invest Ophthalmol Vis Sci. 2010; 51:701–7. [PubMed: 19696177]

Mandal MN, Patlolla JM, Zheng L, Agbaga MP, Tran JT, Wicker L, Kasus-Jacobi A, Elliott MH, Rao CV, Anderson RE. Curcumin protects retinal cells from light-and oxidant stress-induced cell death. Free Radic Biol Med. 2009; 46:672–9. [PubMed: 19121385]

Markovets AM, Fursova AZ, Kolosova NG. Therapeutic Action of the Mitochondria-Targeted Antioxidant SkQ1 on Retinopathy in OXYS Rats Linked with Improvement of VEGF and PEDF Gene Expression. PLoS ONE. 2011; 6:e21682. [PubMed: 21750722]

Minassian DC, Reidy A, Lightstone A, Desai P. Modelling the prevalence of age-related macular degeneration (2010–2020) in the UK: expected impact of anti-vascular endothelial growth factor (VEGF) therapy. Br J Ophthalmol. 2011; 95:1433–6. [PubMed: 21317425]

Preibisch S, Saalfeld S, Tomancak P. Globally optimal stitching of tiled 3D microscopic image acquisitions. Bioinformatics. 2009; 25:1463–5. [PubMed: 19346324]

Qi X, Lewin AS, Hauswirth WW, Guy J. Optic neuropathy induced by reductions in mitochondrial superoxide dismutase. Invest Ophthalmol Vis Sci. 2003:44. [PubMed: 12506054]

Rohrer B, Long Q, Coughlin B, Wilson RB, Huang Y, Qiao F, Tang PH, Kunchithapautham K, Gilkeson GS, Tomlinson S. A targeted inhibitor of the alternative complement pathway reduces angiogenesis in a mouse model of age-related macular degeneration. Invest Ophthalmol Vis Sci. 2009; 50:3056–64. [PubMed: 19264882]

Rudnicka AR, Jarrar Z, Wormald R, Cook DG, Fletcher A, Owen CG. Age and Gender Variations in Age-related Macular Degeneration Prevalence in Populations of European Ancestry: A Meta-analysis. Ophthalmology. 2011; 119:571–80. [PubMed: 22176800]

Rudolf M, Malek G, Messinger JD, Clark ME, Wang L, Curcio CA. Sub-retinal drusenoid deposits in human retina: organization and composition. ExpEye Res. 2008; 87:402–8.

Sandbach JM, Coscun PE, Grossniklaus HE, Kokoszka JE, Newman NJ, Wallace DC. Ocular pathology in mitochondrial superoxide dismutase (Sod2)-deficient mice. Invest Ophthalmol Vis Sci. 2001; 42:2173–8. [PubMed: 11527927]

Seddon JM, Ajani UA, Sperduto RD, Hiller R, Blair N, Burton TC, Farber MD, Gragoudas ES, Haller J, Miller DT. Dietary carotenoids, vitamins A, C, and E, and advanced age-related macular degeneration. Eye Disease Case-Control Study Group. JAMA. 1994; 272:1413–20. [PubMed: 7933422]

Shen JK, Dong A, Hackett SF, Bell WR, Green WR, Campochiaro PA. Oxidative damage in age-related macular degeneration. Histol Histopathol. 2007; 22:1301–8. [PubMed: 17701910]

Smith RT, Chan JK, Busuoic M, Sivagnanavel V, Bird AC, Chong NV. Autofluorescence characteristics of early, atrophic, and high-risk fellow eyes in age-related macular degeneration. Invest Ophthalmol Vis Sci. 2006; 47:5495–504. [PubMed: 17122141]

Sohrab MA, Smith RT, Salehi-Had H, Sadda SR, Fawzi AA. Image registration and multimodal imaging of reticular pseudodrusen. Invest Ophthalmol Vis Sci. 2011; 52:5743–8. [PubMed: 21693600]

Swaroop A, Chew EY, Bowes Rickman C, Abecasis GR. Unraveling a Multifactorial Late-Onset Disease: From Genetic Susceptibility to Disease Mechanisms for Age-Related Macular Degeneration. Annu Rev Genomics Hum Genet. 2009 epub 2009.

Tanito M, Agbaga MP, Anderson RE. Upregulation of thioredoxin system via Nrf2-antioxidant responsive element pathway in adaptive-retinal neuroprotection in vivo and in vitro. Free Radic Biol Med. 2007; 42:1838–50. [PubMed: 17512463]

Tee LBG, Penrose MA, O'Shea JE, Lai CM, Rakoczy EP, Dunlop SA. VEGF-induced choroidal damage in a murine model of retinal neovascularisation. Br J Ophthalmol. 2008; 92:832–8. [PubMed: 18523088]

Thampi P, Rao HV, Mitter SK, Cai J, Mao H, Li H, Seo S, Qi X, Lewin AS, Romano C, Boulton ME. The 5HT(1a) Receptor Agonist 8-Oh DPAT Induces Protection from Lipofuscin Accumulation and Oxidative Stress in the Retinal Pigment Epithelium. PLoS ONE. 2012; 7:e34468. [PubMed: 22509307]

Thurman JM, Renner B, Kunchithapautham K, Ferreira VP, Pangburn MK, Ablonczy Z, Tomlinson S, Holers VM, Rohrer B. Oxidative Stress Renders Retinal Pigment Epithelial Cells Susceptible to Complement-mediated Injury. J Biol Chem. 2009; 284:16939–47. [PubMed: 19386604]

Totan Y, Yagci R, Bardak Y, Ozyurt H, Kendir F, Yilmaz G, Sahin S, Sahin TU. Oxidative macromolecular damage in age-related macular degeneration. Curr Eye Res. 2009; 34:1089–93. [PubMed: 19958129]

Turrens JF, Boveris A. Generation of superoxide anion by the NADH dehydrogenase of bovine heart mitochondria. Biochem J. 1980; 191:421–7. [PubMed: 6263247]

Zhao C, Yasumura D, Li X, Matthes M, Lloyd M, Nielsen G, Ahern K, Snyder M, Bok D, Dunaief JL, LaVail MM, Vollrath D. mTOR-mediated dedifferentiation of the retinal pigment epithelium initiates photoreceptor degeneration in mice. J Clin Invest. 2011; 121:369–83. [PubMed: 21135502]

Zhao Z, Chen Y, Wang J, Sternberg P, Freeman ML, Grossniklaus HE, Cai J. Age-Related Retinopathy in NRF2-Deficient Mice. PLoS ONE. 2011; 6:e19456. [PubMed: 21559389]

Zweifel SA, Imamura Y, Spaide TC, Fujiwara T, Spaide RF. Prevalence and significance of subretinal drusenoid deposits (reticular pseudodrusen) in age-related macular degeneration. Ophthalmology. 2010; 117:1775–81. [PubMed: 20472293]

Highlights

- We used created a mouse model with increased oxidative stress in the retinal pigment epithelium caused by knockdown of MnSOD.
- Mice exhibit fundus abnormalities reminiscent of pigmentary changes in dry AMD.
- Optical coherence tomography reveals sub-retinal and sub-RPE hyper-reflective lesions
- Microscopy reveals dystrophic RPE and central retinal atrophy

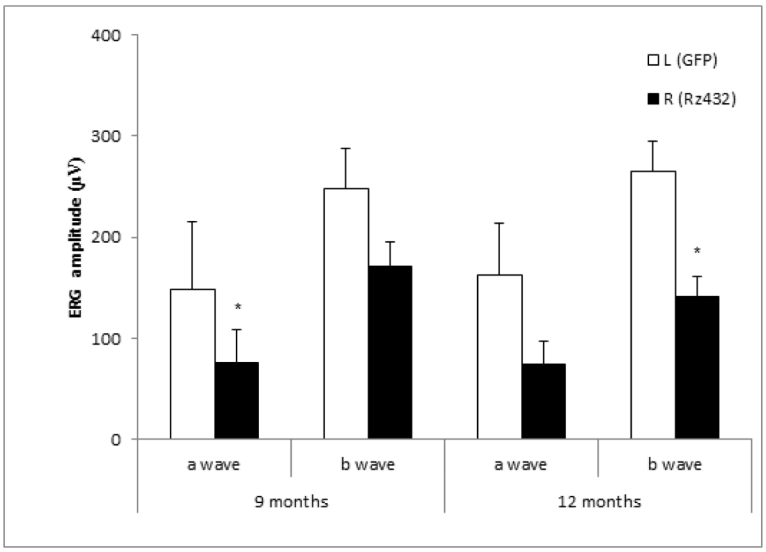

Fig. 1.

Scotopic electroretinogram (ERG) amplitudes decrease following subretinal injection of AAV-SOD2 Rz432. Scotopic full-field ERGs of C57BL/6 mice injected with AAV1-VMD2-Rz432 or AAV-GFP control vector. ERGs were measured at 9 and 12 months post injection. Mice treated with Rz432 showed loss of ERG a-wave response that was significant at both time points and a decrease in the b-wave response that was significant at 12 months. Note: Different cohorts of mice were used at the two intervals. n= 5 at 9 months post injection and n= 10 at 12 months * = $p<0.05$,). Error bars represent standard error of the mean.

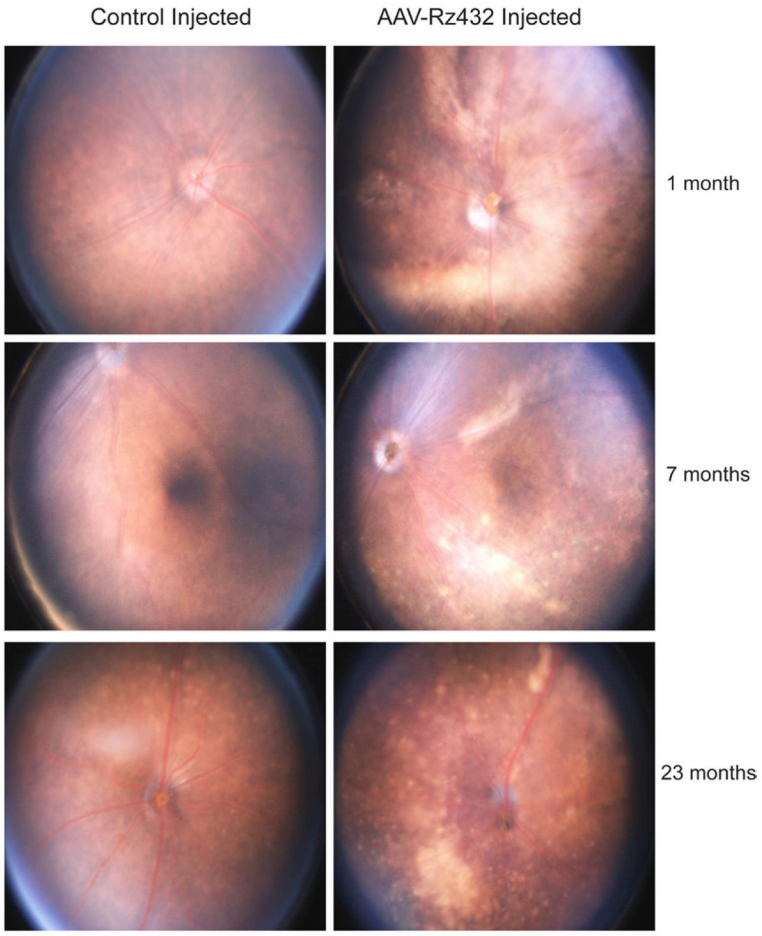

Fig. 2.

Funduscopic changes of Rz432-injected eyes. Hypopigmented regions of the enteral retina were observed as early as one month post injection of AAV-VMD2-Rz432, but not in control injected eyes. At later time points both regions of pigment loss, often in regions underlying the vasculature, and discrete punctate deposits were observed.

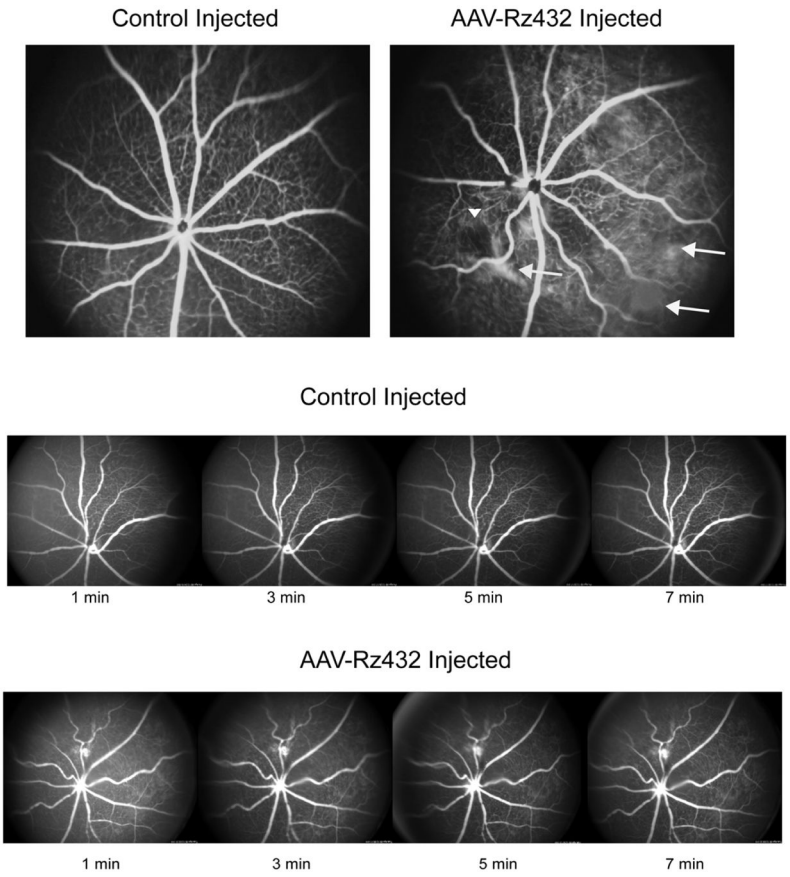

Fig. 3.

Vascular abnormalities revealed by fluorescein angiography. Top. Fluorescein angiography was performed 10 min post injection of fluorescein. Increased tortuosity of retinal blood vessels was observed by seven months and areas of diffuse fluorescence suggested hemorrhaging. However, time-lapse imaging (bottom) indicated no change in the fluorescence pattern with time, indicating that the diffuse fluorescence was not caused by an active hemorrhage, but perhaps by scarring.

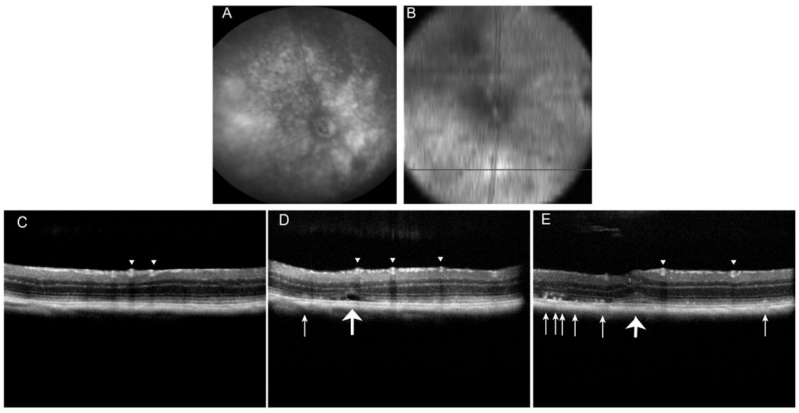

Fig. 4.

SD-OCT imagining reveals subretinal deposits of undefined origin in eyes treated with AAV-Rz432. (A) Digital fundus image of retina taken at 12 months post injection. (B) An *en face* SD-OCT image of the deeper layer of the same retina made at the same time. (C–D) B-scans taken at the position in the retina indicated by the black line in (B). The arrowheads point to retinal blood vessels and the small arrows point to subretinal hyper-reflective material. The large arrow in (D) points to what may be a fluid filled space beneath the retina and the large arrow in (E) indicates a deformation affecting both outer and the inner retina.

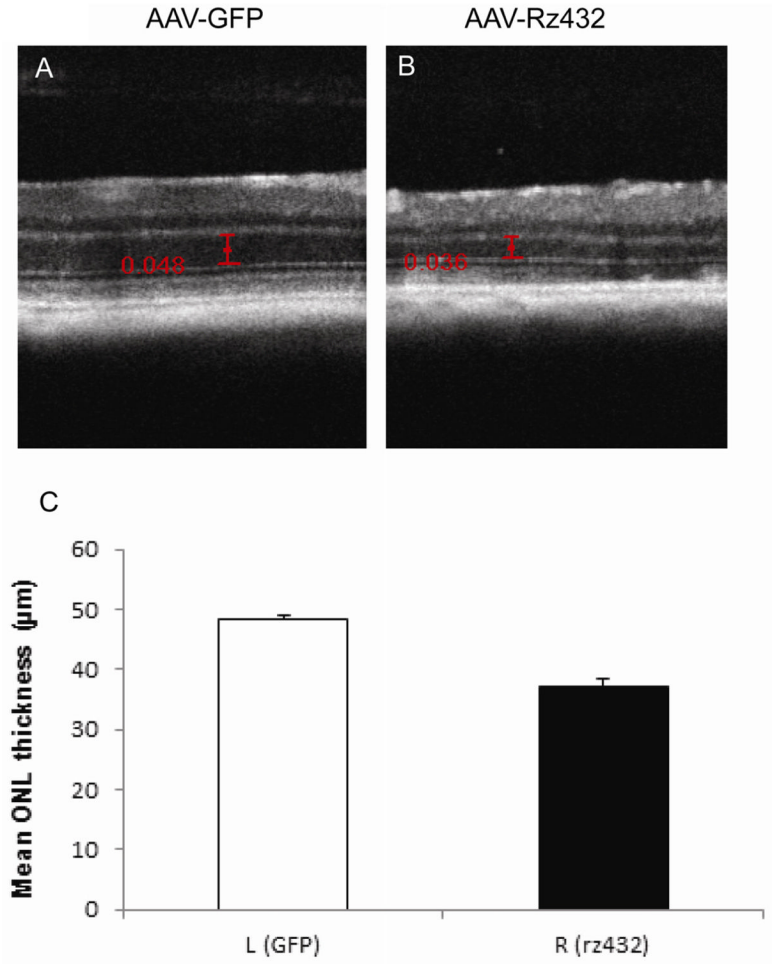

Fig. 5.

Thinning of the ONL revealed by SD-OCT. (A) SD-OCT b-scan of the central retina in an eye 12 months after injection with AAV-GFP. Calipers are in millimeters. (B) A similar scan in an eye 12 months after treatment with AAV-VMD2-Rz432. This is the contralateral eye of the same mouse. (C) Mean ONL thickness measured in six mice, left eyes treated with AAV-GFP, and right eyes treated with AAV-VMD2-Rz432 (**p<0.001).

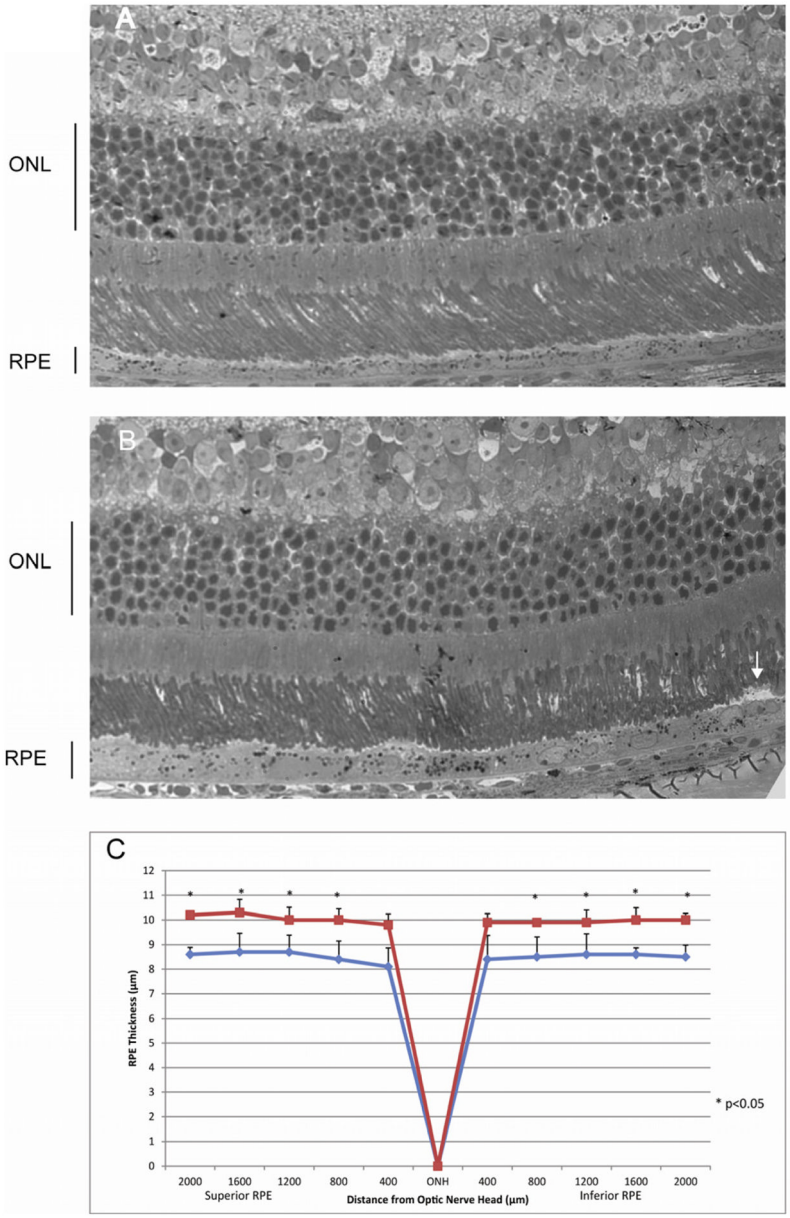

Fig. 6.

Subretinal deposit and thickening of the RPE in eyes treated with AAV-*VMD2*-Rz432. At 7 months post injection, AAV-GFP treated eyes and AAV-*VMD2*-Rz432, were fixed with glutaraldehyde, dehydrated and embedded in epoxy resin. The thickness of the the RPE layer was measured along the vertical meridian by an investigator who did not know the treatment group. (A) Retina treated with AAV-GFP; (B) Retina treated with AAV-*VMD2*-Rz432; the arrow indicates a subretinal deposit. (C) Measurement of RPE thickness at 10 locations equally spaced relative to the optic nerve head (ONH) n=4, *=p<0.05. Squares= AAV-*VMD2*-Rz432 eyes; diamonds=AAV-GFP treated eyes.

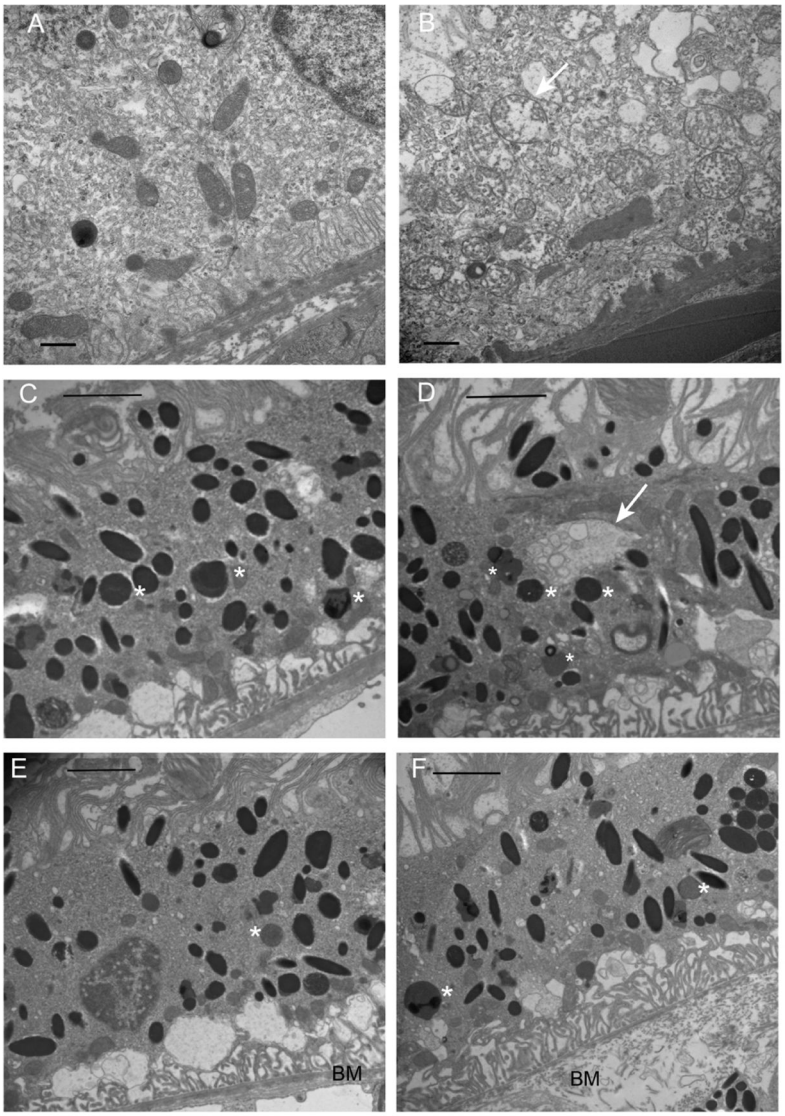

Fig. 7.

Mitochondrial damage and Bruch's membrane injury following knockdown of MnSOD. (A) Image from the AAV-GFP injected eye, 7 months post injection. (B) The AAV-*VMD2*-Rz432 injected eye of the same mouse. In regions of *VMD2*-Rz432 transduction, we noted increase vacuolization of the RPE (this can also be seen in the light micrographs), thickening and disorganization of Bruch's membrane (BM), and distension and loss of cristae from mitochondria (arrow). The scale bar is 500 nm. In both AAV-GFP treated eyes (C) and AAV-Rz432 treated eyes (D), we observed lipofuscin granules (marked with asterisks), but in the ribozyme-treated eyes we frequently observed autophagosomes containing vesicles (arrow in D). In ribozyme treated eyes (F), Bruch's membrane (BM) was typically distended and lacking in its normal laminar organization compared to control injected retinas (E).

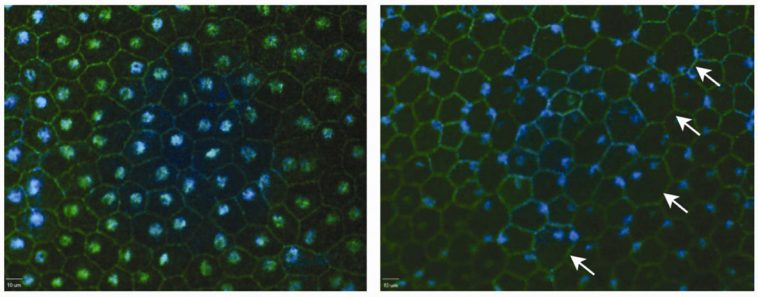

Fig. 8.

Nucelar dislocation in the RPE following delivery of AAV-*VMD2*-Rz432. RPE flat mounts were stained using antibody to ZO1 and DAPI. RPE derived from Rz432 treated eye (right) showed enlarged cells (arrows), an increased number of binucleated cells and displacement of nuclei to the periphery of cells (blue: DAPI, green: ZO1). These are from the left and right eyes of the same mouse.

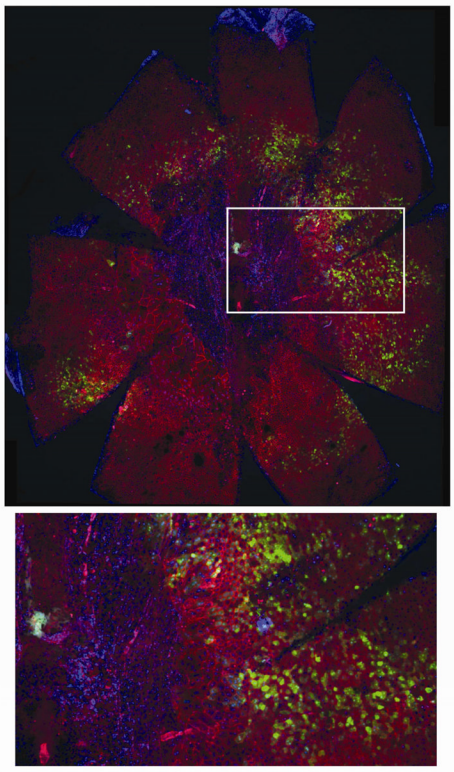

Fig. 9.

MnSOD knockdown leads to central fibrosis and irregular RPE morphology. RPE flat mounts were prepared 23 months after injection of AAV-*VMD2*-Rz432. **Top:** 48 RGB confocal stacks were made at an original magnification of 10X merged and stitched together using Fiji software. Large irregular cells and RPE atrophy (loss of phalloidin-stained boundaries) are apparent with concomitant appearance of closely packed nuclei, presumably fibrotic cells. **Bottom:** enlargement of the boxed region, possibly indicating fibrosis surrounding the optic nerve head, with an adjacent transitional zone containing enlarged, irregular and multinucleate RPE cells. Interestingly, surrounding RPE cells appear normal, even though some cells express GFP derived from the AAV vector (Supplemental Fig. 1), and this was confirmed by scanning confocal microscopy (data not shown).